electronics

MDPI

Review

A Review of Advanced Antennas with Experimental Ground-Penetrating Radar Applications

Abdelhalim Chaabane [1], Djelloul Aissaoui [2], Lakhmissi Cherroun [3] and Giovanni Angiulli [4,*]

[1] Department of Electronics, Faculty of Technology, University of Ferhat Abbas Setif-1, Setif 19000, Algeria; abdelhalim.chaabane@univ-setif.dz
[2] Telecommunications and Smart Systems Laboratory, University of Djelfa, P.O. Box 3117, Djelfa 17000, Algeria; djelloul.aissaoui@univ-djelfa.dz
[3] Applied Automation and Industrial Diagnostics Laboratory, Faculty of Sciences and Technology, University of Djelfa, Djelfa 17000, Algeria; l.cherroun@univ-djelfa.dz
[4] DIIES Department, Mediterranea University, Via Zehender, 89122 Reggio Calabria, Italy
* Correspondence: giovanni.angiulli@unirc.it

Abstract

Ground-Penetrating Radar (GPR) serves as an essential non-destructive tool for subsurface exploration, and its antenna system largely determines the performance of the overall system. This paper presents a comprehensive review of advanced GPR antenna technologies, examining six major types: Vivaldi, bowtie, tapered, dipole, envelope, and spiral. This analysis shows that trade-offs among these antennas are unavoidable. High-frequency wideband antennas deliver high gain, but their penetration depth is limited to very shallow targets. Some wideband designs achieve wide bandwidth and reasonable gain with compact footprints, while others are suited for detecting embedded metallic objects. By comparison, low-frequency designs operating in the VHF and UHF bands enable very deep penetration, making them suitable for detecting deeply buried targets in lossy media and subsurface utilities. However, deep penetration often comes at the cost of lower gain or larger physical size. Ultimately, no universal antenna exists; the optimal choice depends on whether depth, resolution, or adaptability to attenuating environments is prioritized. Emerging metasurface-integrated and frequency-selective surface (FSS)-backed antennas represent a promising frontier, enabling better bandwidth, gain, and compactness. Ongoing challenges include miniaturization without compromising performance, reliable operation in heterogeneous and lossy soils, and the development of robust, manufacturable designs for field deployment. This review offers researchers and practitioners a structured reference, guiding the development of next-generation GPR systems that balance deeper penetration, higher resolution, and operational versatility.

Keywords: ground-penetrating radar (GPR); Vivaldi antenna; bowtie antenna; dipole antenna; envelope antenna; tapered antenna; spiral antenna; ultra-wideband (UWB); frequency selective surfaces (FSSs)

Academic Editor: Reza K. Amineh

Received: 29 April 2026
Revised: 24 May 2026
Accepted: 29 May 2026
Published: 1 June 2026

1. Introduction

Ground-Penetrating Radar (GPR) has become a key non-invasive sensing technology for subsurface exploration, with wide-ranging applications in geology, mineral exploration, glaciology, civil engineering, geophysics, archaeology, environmental monitoring, infrastructure diagnostics, and more [1–6]. By transmitting electromagnetic waves into the ground and analyzing the reflected signals from buried objects and material discontinuities,

GPR systems enable accurate detection and imaging without destructive intervention [7,8]. Despite these advantages, the overall performance of a GPR system is strongly dependent on the design and efficiency of its antenna subsystem [9]. The antenna is the most critical component in GPR systems, as it directly governs essential performance parameters such as bandwidth, radiation characteristics, resolution, and penetration depth [10,11]. A central challenge in antenna design for GPR lies in managing the inherent trade-off between high-resolution imaging and sufficient penetration depth. High-frequency signals provide finer resolution but experience rapid attenuation in lossy media, whereas low-frequency signals penetrate deeper but offer reduced imaging detail [12]. Achieving an optimal balance between these competing requirements remains a fundamental objective in GPR antenna development. The operating sequence of a typical GPR system is shown in Figure 1, which illustrates how electromagnetic waves are transmitted, reflected from subsurface interfaces, and received to detect buried objects. For underground object detection, the antenna system must efficiently couple electromagnetic energy into the soil. Unlike free space propagation, the air–soil interface introduces a significant impedance mismatch due to dielectric discontinuities. Wideband antennas improve broadband impedance matching and enable efficient transmission over a wide frequency range. Polarization also affects target detectability: linearly polarized antennas produce stronger responses from elongated targets aligned with the electric-field direction, while dual-polarized configurations improve detection of targets with arbitrary orientations. Therefore, the operating principle relies on broadband operation, impedance matching, and polarization diversity to balance penetration capability and resolution. The process begins in the control unit, which supplies power and manages signal processing and display. The transmitter system generates short, high-frequency pulses using a pulse generator, and these pulses are radiated into the ground through the transmitting antenna as incident electromagnetic waves. As these waves propagate through the subsurface, their velocity and behavior depend on the electrical properties of the materials encountered, such as permittivity and conductivity. When the waves reach a boundary between different materials—such as soil and a buried object like a rock or pipe—a portion of the energy is reflected back toward the surface while the rest continues deeper. The receiver system captures these reflected signals using a receiving antenna, after which they are amplified by a low-noise amplifier to preserve signal integrity and then processed to extract meaningful information. By measuring the time delay between the transmitted pulse and the received echo, the system can estimate the depth and position of the buried object, while the signal amplitude provides insight into its material properties. The processed data is finally displayed as a subsurface image or radargram, enabling visualization and interpretation of underground features [13–15]. Designing GPR antennas involves several inherent trade-offs. Higher frequencies experience greater attenuation when penetrating the ground or walls, so most systems operate at relatively low frequencies to achieve deeper penetration. However, high-resolution imaging demands a wide operational bandwidth. The combination of a low center frequency with a wide bandwidth makes GPR antenna design particularly challenging [16]. Lower frequencies enable deeper penetration but provide coarser resolution, whereas higher frequencies deliver finer resolution at the expense of shallower depth. Consequently, low-frequency antennas are larger in size, while high-frequency antennas are smaller [17,18]. Beyond frequency selection, the antenna's electromagnetic performance fundamentally governs system effectiveness. Wide bandwidth directly shortens time-domain pulses, improving the ability to resolve closely spaced features [19]. High gain combined with directional broadside radiation increases penetration depth and mitigates signal attenuation at higher frequencies. Stable, well-defined radiation patterns further enhance detection and imaging accuracy [20].

Higher gain also extends the system's effective range and can reduce transmitter power requirements [21].

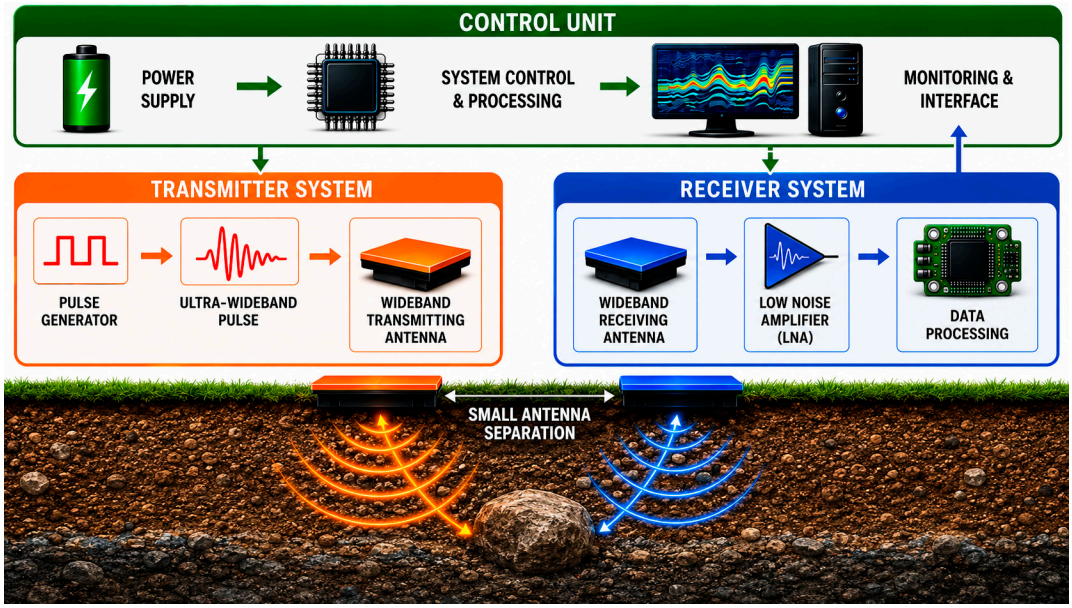

Figure 1. Schematic Diagram of a GPR System for Subsurface Detection.

Nevertheless, achieving high gain in compact, wideband antennas remains challenging, particularly at lower frequencies where size inherently increases—a critical constraint for portable or vehicle-mounted GPR systems. Over the past few decades, continuous efforts have improved conventional GPR antenna designs. Well-established geometries such as Vivaldi, bowtie, tapered, monopole, dipole, spiral, and envelope antennas are widely studied for their broadband behavior, structural simplicity, and subsurface sensing suitability [22]. Among these, Vivaldi and bowtie antennas offer ultra-wideband operation and stable radiation patterns, enabling high-resolution imaging. Bowtie designs, in particular, benefit from cavity or reflector structures that enhance a front-to-back ratio [23–25]. Compared with the bowtie antennas, the tapered slot antenna has the properties of directional radiation, broader band and higher gain [26]. Planar UWB antennas are preferred for lower-frequency operation since GPR penetration depth degrades at higher frequencies. To improve depth resolution, a reflecting screen placed below the antenna directs waves toward the broadside direction, enhancing gain—metallic reflectors are particularly effective for this purpose [27]. In GPR systems, backward radiation (directed away from the ground) is wasted. To mitigate this, a shielded cavity or metal reflector is conventionally placed behind antennas with omnidirectional patterns to redirect backward energy toward the forward direction, thereby improving directional gain. This backside loading technique is particularly effective at high operating frequencies, where the short wavelength allows the cavity or reflector height to remain practically small [28,29].

Dipole antennas are valued for ease of implementation and flexibility. Spiral antennas, including the planar Archimedean configuration, provide frequency-independent operation, high efficiency, low profile, stable impedance, and circular polarization [30]. Envelope antennas have demonstrated compact size and improved transient response, which are advantageous for time-domain GPR systems [31]. Collectively, these antenna families offer a rich design space for achieving high range resolution and deep target detection in GPR applications. Despite the maturity of these antenna types, ongoing research continues to introduce new structures, geometrical modifications, and design strategies aimed at enhancing their performance. These advancements include bandwidth enhancement tech-

niques, size reduction approaches, gain and directivity improvements, and optimization for operation in complex and lossy subsurface environments [32]. In this context, this paper presents a comprehensive review of the most recent advanced antenna designs reported in the literature with experimental GPR applications, focusing specifically on structural advancements published during the last five years. The antenna types covered include Vivaldi, bowtie, tapered, dipole, spiral, and envelope antennas. By integrating recent design innovations with emerging approaches and intelligent methodologies, this review aims to provide a clear and holistic understanding of the current state of the art in GPR antenna technology, thereby supporting future innovations in subsurface sensing applications.

This paper is organized as follows. Section 2 presents recent design advancements across all considered antenna types, including Vivaldi, bowtie, dipole, envelope, tapered, and spiral, with emphasis on their performance improvements, suitability for subsurface sensing applications, and limitations. Finally, Section 3 provides a comparative analysis of these antenna categories, identifying key trade-offs, strengths, and suitability. In accordance with copyright policies, only figures from articles published under a Creative Commons Attribution (CC BY) license are included in this review. Figures from other publications are not reproduced; however, their key results are summarised in the text, and the reader is referred to the original references for further details.

2. Recent Antenna Designs with Experimental GPR Applications

2.1. Vivaldi Antennas

Vivaldi antennas are well-suited for GPR applications because they provide stable ultra-wideband (UWB) directivity and high resolution within a compact form factor [33]. Building on this design, the antipodal Vivaldi antenna enables further miniaturization while maintaining wideband performance and high gain (>6 dBi) [8]. Consequently, key advantages include ultra-wide bandwidth (>105%), end-fire radiation, low dispersion, and low-cost planar fabrication [33]. For instance, a compact dual-polarized UWB antipodal Vivaldi antenna arranged in a box configuration using four single-polarized elements achieves an operating bandwidth from 0.3 GHz to 3 GHz with a low-profile design, making it well-suited for rover-based polarimetric GPR systems [34], while another miniaturized low-profile ultra-wideband antipodal Vivaldi antenna array loaded with edge techniques covers 0.9–12 GHz with wide-angle scanning [35].

Despite these merits, several drawbacks persist, namely, gain-bandwidth trade-offs, pattern instability, and large physical size at lower frequencies. To address these limitations, researchers have explored various advanced strategies, leading to a series of innovative designs that extend the capabilities of Vivaldi antennas for specific GPR scenarios. For example, integrating frequency-selective surfaces (FSS) into the antenna aperture produced a design with a reported gain of 13.6 dBi within the critical 0.6–4 GHz band, a significant improvement for many GPR tasks. Similarly, employing a partially dielectric-loaded planar Vivaldi array enabled operation down to 380 MHz, a crucial frequency range for deeper subsurface exploration [36]. Another innovative approach uses slow-wave structures and resistive loading to achieve an electrically highly compact UWB Vivaldi antenna, which has been successfully validated for detecting buried rebar in GPR imaging experiments. Therefore, despite the remaining challenges, the continued evolution of Vivaldi antennas and their variants—including dual-polarized designs for rover-based systems—ensures they remain promising for GPR due to their broadband matching, unidirectional radiation, and compactness [37,38]. Building on these advances, several recent studies have introduced Vivaldi-based antennas with enhanced polarization control or improved low-frequency matching. Although the original figures from these works are not reproduced here due to copyright restrictions, their key findings are summarized below, and the reader is referred

to the original sources [39,40] for the complete graphical content. First, a dual-band circularly polarized (CP) antipodal Vivaldi antenna for GPR and satellite applications was presented in [39]. Unlike conventional designs, it uses a single-layer FSS metasurface polarizer to convert linear to circular polarisation at 6.4–7.6 GHz and 15.2–16.2 GHz, achieving an ultra-wide impedance bandwidth (1.7–40 GHz) and broadside radiation. Experimental tests at 1- to 2-inch soil depths successfully detected buried metal sheets, where the clarity of the hyperbolic response confirmed proper target identification. However, the antenna has limitations: verification was restricted to shallow depths and metal targets, and the non-uniform FSS metasurface adds fabrication complexity and alignment sensitivity. The shallow depth constraint arises because soil attenuation increases with depth, limiting the effective range. While the previous design focused on circular polarization, other researchers have pursued compact impedance matching techniques to enhance low-frequency performance. Again, the original figure is not reproduced here, so the following summary relies on the description in [40].

A representative example is a compact coplanar waveguide (CPW)-fed Vivaldi antenna with an integrated single-stub matching technique, where the stub position is optimized to improve low-frequency impedance matching for GPR applications [40]. Fabricated on an FR-4 substrate ($80 \times 80 \times 1.635$ mm^3), the antenna achieves measured broadband operation from 1.13 to 5 GHz, a peak gain of 10.36 dBi at 1.9 GHz, a radiation efficiency of approximately 90.16%, and a return loss of -39.13 dB at resonance. To validate its practical utility, a sandbox GPR experiment was conducted using a bistatic configuration. The resulting A-scan profile (see the original paper [40] for the plot) displays the envelope amplitude as a function of depth. A distinct peak appears at an estimated depth of 377 mm, which closely corresponds to the actual burial depth of 400 mm. The small discrepancy of 2.3 cm can be attributed to uncertainty in the dielectric constant of the sand and residual timing offsets. Overall, these results demonstrate that the proposed antenna and method can successfully detect buried metallic objects and provide reasonable depth estimation, thereby validating their effectiveness for practical GPR applications. Nevertheless, several limitations should be acknowledged. First, the sandbox test represents a preliminary, controlled environment and does not fully replicate real field conditions. Second, no validation has yet been performed in more realistic GPR scenarios, such as lossy or heterogeneous soils. Addressing these weaknesses will be an important direction for future work. Beyond single-polarization and stub-tuned designs, full polarimetric capability has been achieved through compact dual-polarised Vivaldi configurations, as illustrated in the following two examples, where permission to reproduce the figures has been obtained. As illustrated in Figure 2, a compact UWB dual-polarised Vivaldi antenna for full polarimetric GPR applications is presented in [41]. The design employs a shared aperture configuration with four obliquely arranged Vivaldi elements and a square loop reflector, achieving orthogonal polarizations, enhanced low-frequency gain, and low dispersion. The fabricated antenna offers an impedance bandwidth of 0.4–4.0 GHz (164% fractional bandwidth), port isolation >40 dB, and a gain of 4–12 dBi within a compact form factor of $0.28\lambda \times 0.28\lambda \times 0.20\lambda$ at the lowest operating frequency. A compact GPR testbed ($1200 \times 800 \times 400$ mm^3) filled with Singaporean-approved soil mix ($\varepsilon_r \approx 28 - j2.5$) was used. Two dual-polarized Vivaldi antennas (TX/RX) were placed side by side 10 cm apart, 6 cm above the soil, and operated from 0.4 to 3.0 GHz using a VNA. A metal rebar buried at a depth of 9 cm was scanned with a 2 cm step, and B-scan data were processed by background removal, successfully revealing the hyperbolic signature of the target. However, several limitations are evident. First, the experimental validation was conducted in a static ground-based testbed rather than on an actual airborne platform. Second, the challenging soil environment—characterized by high

moisture, conductivity, and heterogeneity—introduced clutter from the rough soil surface, stones, and wet clods, which led to residual noise in the B-scan images.

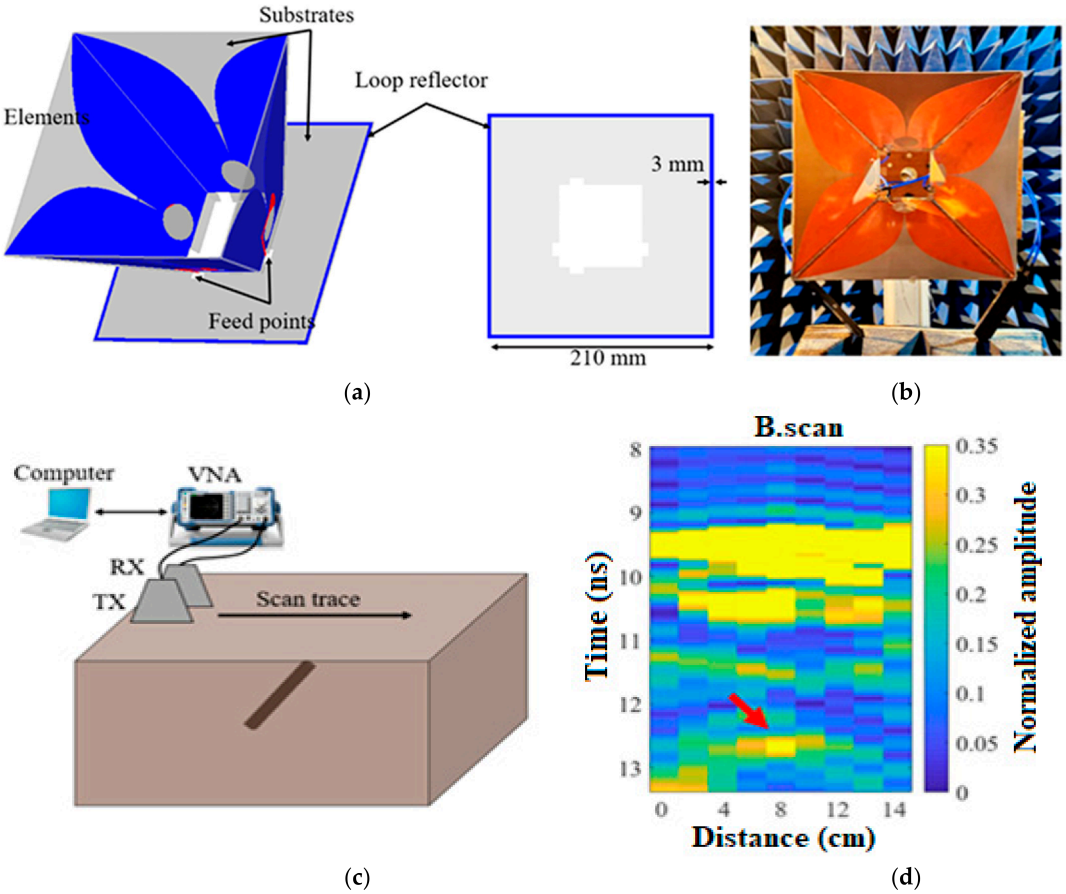

Figure 2. (**a**) Geometry of the proposed dual-polarized Vivaldi antenna; (**b**) fabricated prototype; (**c**) illustration of the experimental bistatic GPR system; (**d**) B-scan data with time (ns) versus normalized amplitude, and distance (cm) along the scan trace. Reproduced from [41] (Copyright © 2021 H.H. Sun et al.). This figure is licensed under the Creative Commons Attribution 4.0 International License (CC BY). It has undergone minor technical enhancements in terms of clarity and legibility to meet journal standards. These modifications do not alter the original scientific content or data representation. For the full license terms, see https://creativecommons.org/licenses/by/4.0/ (accessed on 28 May 2026).

The same dual-polarized Vivaldi concept has also been adapted to non-traditional GPR applications, such as tree trunk defect imaging. This is shown in Figure 3, which presents a compact dual-polarized Vivaldi antenna system for tree radar applications [42]. The design employs a shared aperture configuration with two orthogonal pairs of Vivaldi elements, each incorporating planar directors and edge slots to enhance gain while maintaining broad bandwidth; a metal back reflector further improves gain and suppresses back-lobes. The fabricated antenna operates from 0.5 GHz to 3 GHz with a compact form factor of $0.29\lambda \times 0.29\lambda \times 0.48\lambda$ at the lowest frequency, achieving a gain of 5.5–14.8 dBi and cross-polarization discrimination exceeding 20 dB. Validation through tree trunk defect imaging was performed via a contactless measurement on a rain tree trunk (30 cm diameter) with a 6 cm cavity buried 5 cm from the center. The B-scans and migrated images obtained by the proposed antenna yielded a clearer hyperbolic signature and a distinguishable cavity region. Nevertheless, several limitations are noted. First, the detection capability varies with antenna–trunk distance, which is a relationship that was not investigated. Second,

the high-humidity environment (Singapore) resulted in elevated wood permittivity and conductivity, which may limit generalizability to drier climates.

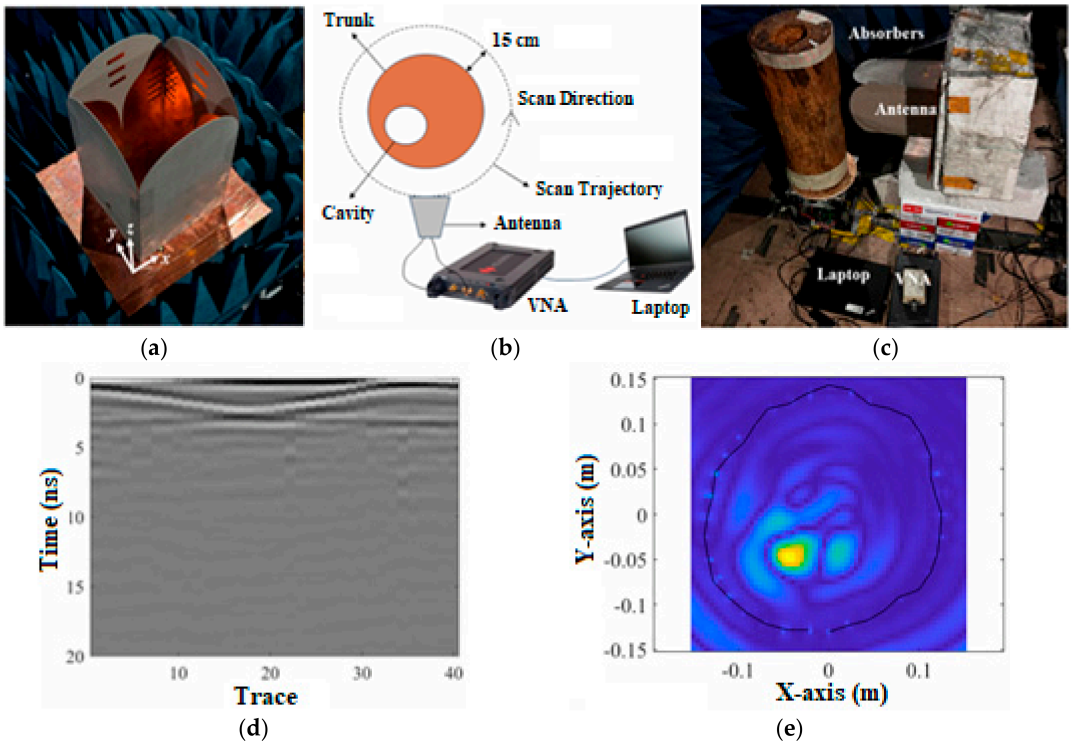

Figure 3. (**a**) Photograph of the fabricated shared aperture antenna system; (**b**) measurement setup for tree trunk scanning; (**c**) schematic block diagram of the setup; (**d**) measured raw B-scans; (**e**) migrated B-scan. Reproduced from [42] (Copyright © 2024 K. Cheng et al.). This figure is licensed under the Creative Commons Attribution 4.0 International License (CC BY). It has undergone minor technical enhancements in terms of clarity and legibility to meet journal standards. These modifications do not alter the original scientific content or data representation. For the full license terms, see https://creativecommons.org/licenses/by/4.0/ (accessed on 28 May 2026).

2.2. VHF/UHF Antennas: Bowtie, Dipole, and Envelope

Bowtie antennas are widely used in GPR systems due to their low profile, simple feeding, good phase stability, minimal dispersion, and low ringing—especially with resistive loading. As a broadband variant of the dipole, the bowtie achieves a wide impedance bandwidth (up to 10:1) through traveling wave behavior governed by flare angle and arm length. However, typical gain is below 4 dBi, bidirectional radiation wastes energy, and resistive loading reduces radiation efficiency [43,44]. To address these limitations, an acorn-shaped bent folded bowtie antenna (FBA) with a back cavity is proposed in [45] (see Figure 4). The design integrates an arc-shaped distributed multilayer capacitive loading structure combined with resistive loading to enhance low-frequency bandwidth and radiation efficiency. A novel cavity groove reflector ensures tight coupling with the radiator, achieving unidirectional radiation and miniaturization. The antenna achieves a compact electrical size of $0.25\lambda \times 0.15\lambda \times 0.125\lambda$ (at the lowest operating frequency) and operates from 250 MHz to 850 MHz, which spans both the VHF (very high frequency) and UHF (ultra-high frequency) bands, with a simulated bandwidth extending from 100 MHz to 1.1 GHz. It attains a peak radiation efficiency of 50% and a realized gain of 4 dBi at 850 MHz, with a narrow pattern across the band. For measurement, two configurations were used. In basic radiation and time-domain characterization, a wideband balun feeds the antenna under test (AUT), placed 2 m from a square copper-clad laminate (CCL) target. A pulse generator (model GZ1120ME-04, produced by Geozondas, Vilnius, Lithuania) produces

monocycle pulses centered around 400 MHz (amplitude > ±25 V), which are attenuated and fed to the transmitter. The received echo from the CCL is captured by a Keysight MSOS804A oscilloscope. For integrated GPR testing, a balanced transmitter and receiver replace the balun and pulse source; the transmitter generates unipolar Gaussian pulses up to 40 V. An FPGA-based controller manages the GPR prototype, communicating with a PC for B-scan processing and display. Field tests on a road with buried pipes and in a tunnel lining compare the proposed antenna with a commercial 400 MHz GPR, confirming higher radiation efficiency, deeper detection depth, and clearer B-scan images than conventional resistively loaded designs. Nevertheless, several limitations exist. First, the multilayer capacitive-resistive loading and tightly coupled back cavity increase design complexity and fabrication cost. Second, although electrically compact, the physical dimensions at P-band frequencies remain considerable, limiting deployment in highly space-constrained systems. Third, the narrow beamwidth across the band reduces angular coverage, which may hinder wide-area imaging applications. While the bowtie family provides a solid compromise for moderate depths, certain GPR applications—such as tunnel detection from aerial platforms—require much deeper penetration at even lower frequencies, albeit with different trade-offs in gain and size. In this context, the dipole antenna emerges as a natural alternative. Although no figure is reproduced here due to copyright restrictions, the key findings are summarized below, and the reader is referred to the original source [46] for the complete graphical content.

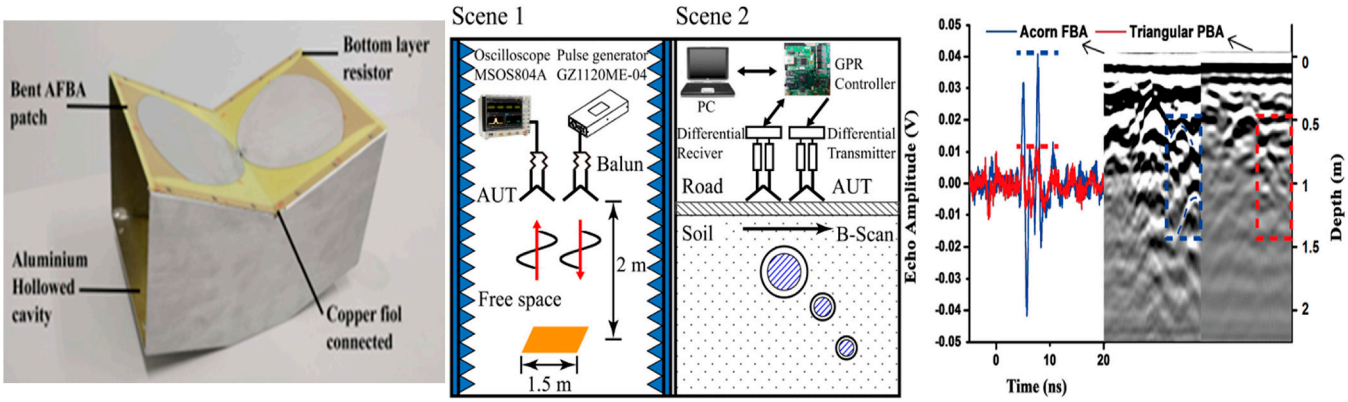

Figure 4. (**a**) Fabricated acorn-shaped folded bowtie antenna (AFBA); (**b**) measurement setup comparing AFBA with a conventional resistively loaded bowtie; (**c**) received echo signals (left: free space echo from copper target showing higher amplitude; right: B-scan from road test showing improved depth and resolution). Reproduced from [45] (Copyright © 2020 G. Yang et al.). This figure is licensed under the Creative Commons Attribution 4.0 International License (CC BY). It has undergone minor technical enhancements in terms of clarity and legibility to meet journal standards. These modifications do not alter the original scientific content or data representation. For the full license terms, see https://creativecommons.org/licenses/by/4.0/ (accessed on 28 May 2026).

To address the stringent demands of autonomous aerial vehicle ground-penetrating radar in the VHF band (30–300 MHz), Ref. [46] proposes an innovative dual H-shaped dipole antenna that achieves substantial improvements in bandwidth and gain while enabling deep subsurface target detection. The antenna operates from 30 to 170 MHz, which falls entirely within the VHF band. The design introduces three key innovations: an RC-loaded folded structure that overcomes narrow-gap fabrication limits at low frequencies by overlapping top–bottom layers; a split director for gain enhancement through in-phase field stacking; and tuning stubs for impedance compensation. As a result, the fabricated prototype achieves $|S_{11}| < -10$ dB from 30 to 170 MHz with a 50 mm profile ($0.017\lambda_0$ at 100 MHz), yielding a 33% bandwidth increase and a 4.2 dB peak gain improvement over a

reference design. When integrated into a 100 MHz-centered GPR system on an autonomous aerial vehicle flying at 30 m altitude, the antenna successfully detected a tunnel buried at 40 m depth. Post-processing gave a calculated depth of 39.9 m (assuming $\varepsilon_r = 4.2$), which closely matches the actual value. Despite these promising results, the proposed design is not without limitations. The inclusion of lumped RC components inevitably increases both design complexity and manufacturing cost. Furthermore, the antenna's performance has yet to be evaluated under realistic operating conditions, including heterogeneous or lossy soils and varying flight parameters, leaving its robustness largely unconfirmed. Another unresolved concern is the potential electromagnetic coupling between the antenna and the autonomous aerial vehicle airframe, which could degrade performance during actual field deployments. When the operating environment becomes highly lossy (e.g., wet soil with high permittivity and conductivity), even well-designed bowtie or dipole antennas may suffer from severe attenuation. In such cases, an envelope-type antenna offers an alternative strategy, trading physical size for improved coupling into lossy media. Again, the original figure is not reproduced here due to copyright, so the following summary relies on the description in [47].

To address the need for deep subsurface imaging of pipes and tunnels in lossy environments, Ref. [47] proposes a low-profile, ultra-wideband directive antenna that operates efficiently below 500 MHz while maintaining a compact form factor. The antenna is designed to operate from 140 to 510 MHz, which spans the upper VHF band (140–300 MHz) and the lower UHF band (300–510 MHz). It consists of a pair of coupled modified envelope elements with differential feeding, which together provide a directive pattern normal to the ground plane over a wide bandwidth. Optimized for operation in proximity to a half-space soil medium to maximize air-to-ground power coupling, the PCB prototype has a height of 153 mm (0.17λ at 325 MHz) and lateral dimensions of 600 mm × 600 mm. Measured reflection coefficients near concrete and wet soil (covered by sand and grass) are better than −9.5 dB across the band, while the simulated realized gain in dry soil exceeds 4.9 dBi over 140–510 MHz. For GPR evaluation, a metallic plate (0.61 m × 0.762 m) was buried at 0.6 m depth in wet lossy soil (18.92% moisture, permittivity 16.4 − j2.4 at 300 MHz). Two antennas with a center-to-center separation of 0.8 m were used to reduce direct coupling. The reflected signals (150–450 MHz) successfully imaged the plate at a measured depth of 0.57 m, with a range resolution of 0.101 m. Although the envelope antenna achieves remarkable penetration in difficult soils, its large lateral dimensions (0.6 m × 0.6 m) make it impractical for portable or drone-mounted applications, highlighting the persistent trade-off between electrical performance and physical compactness in VHF/UHF GPR design.

2.3. Tapered Antennas with FSS Reflector

The effectiveness of FSSs and metasurfaces for GPR antennas arises from three closely related electromagnetic mechanisms: high-impedance boundary behavior, controlled reflection-phase dispersion, and broadband constructive interference. A conventional metallic reflector introduces an approximately 180° phase reversal upon reflection and typically requires a quarter-wavelength air-gap to achieve in-phase addition, which tends to restrict efficient operation to a relatively narrow frequency region [20,27]. In contrast, an FSS composed of sub-wavelength resonant unit cells can be engineered to provide a high-impedance reflection response with a controlled reflection phase over the operating band [48]. The frequency-selective behavior originates from electromagnetic coupling among the periodic unit cells; consequently, conventional FSS structures often require electrically large apertures. However, miniaturized-element FSSs (unit cells typically smaller than λ/10) exhibit effective metamaterial-like behavior, offering reduced sensitivity to incidence and polarization angles while maintaining a compact profile [49]. When posi-

tioned behind a printed UWB antenna, the FSS reflects back-radiated fields so that the reflected and directly radiated waves combine constructively in the broadside (+z) direction, thereby reducing back-lobe radiation while improving gain, directivity, and front-to-back ratio [27,48,50]. In addition, the FSS can provide shielding for nearby electronics and facilitate compact integration near metallic environments [50,51]. Depending on its design, the periodic surface may also operate as a broadband stop-band reflector that suppresses undesired backward propagation and enhances forward radiation through constructive interference [51]. A major advantage of FSS/metasurface reflectors over conventional metallic plates is their engineered reflection-phase response [20]. For a metallic reflector, the reflection phase remains approximately constant near 180°, causing destructive interference except near the frequency where the antenna-to-reflector spacing approaches $\lambda/4$ [20,27]. By contrast, an FSS can be designed so that its reflection phase varies in a controlled and approximately linear manner across the operating band [20]. Under these conditions, the reflected and directly radiated fields remain approximately co-phased over a wider bandwidth, enabling broadband constructive interference, improved beam collimation, and gain enhancement [20] (as frequency increases, the wave closer to the FSS experiences a controlled linear phase decrease [51]). Thus, the purpose of FSS-backed GPR antennas is not only to increase gain, but also to achieve broadband phase compensation, reduced dispersion, improved pulse preservation, and robust angular performance, all of which are important for high-resolution subsurface imaging. Realizing a wideband single-layer FSS with stable reflection-phase characteristics remains challenging; therefore, multilayer structures, miniaturized elements, or resistively loaded configurations are often employed. This principle underlies the antenna in [52], which employs an optimized square-loop FSS with a wide low-dispersion stop-band and resistive loading to suppress cavity resonances. Similar techniques have also been applied to develop compact interdigital FSS designs [52] and to enhance the gain of UWB monopole antennas [53]. The antenna proposed in [54] operates from 0.6 GHz to 4.6 GHz with a peak gain of 7 dBi. The complete structure, including the reflector, measures $18 \times 22 \times 5$ cm^3 and is built using low-cost, lightweight materials to ease fabrication and integration. Performance was validated over sandy soil. The fabricated prototype, experimental setup, and B-scan results are presented in Figure 5, which shows two antennas—one serving as an emitter and the other as a receiver. A clear hyperbolic reflection curve, indicating the detectability of subsurface targets using the proposed antenna pair, is observed and highlighted with a red dashed circle. Nevertheless, the design has practical limitations. Validation was confined to sandy soil, so its performance in other subsurface environments—such as clay, loam, wet soil, or layered strata—remains unconfirmed. Additionally, the optimized periodic reflector increases fabrication complexity and requires more precise alignment than a simple standalone antenna.

2.4. Spiral Antenna

A noteworthy advancement in polarization-diverse GPR antennas is the composite dual-arm spiral antenna, which integrates equiangular and Archimedean structures. As presented in Figure 6, this design was developed in [55] to improve subsurface linear object detection and polarization sensitivity. The antenna operates from 1 to 5 GHz with stable circular polarization (axial ratio < 3 dB). An exponentially tapered balun provides impedance matching, while a metallic-backed cavity with absorbing materials enhances directivity and suppresses back-reflections. In a 3D GPR test, five steel rebars (1 cm diameter, buried 12 cm deep in sand with $\varepsilon_r = 3$) were scanned over a 0.45 m $\times$ 0.5 m area. The spiral antenna clearly imaged all rebars with equal amplitude regardless of their orientation. Despite these advantages, the proposed spiral antenna presents several practical challenges. To begin with, its ability to penetrate lossy soils diminishes significantly at frequencies below

1 GHz, which limits its effectiveness in high-attenuation environments. Moreover, the need for both left-hand and right-hand circularly polarized antennas for the GPR test increases system complexity and overall cost. The inclusion of a metallic cavity and absorbing materials further adds to the device's weight, making it less suitable for lightweight or airborne platforms. In addition, the antenna has not been evaluated on deeper buried targets or in heterogeneous ground conditions, leaving its performance under such scenarios uncertain.

(**a**) (**b**) (**c**)

Figure 5. (**a**) Photograph of the fabricated reflector-backed tapered antenna; (**b**) photograph of the experimental GPR setup; and (**c**) B-scan results from the pulse radar system. Reproduced from [52] (Copyright © 2021 A. Raza et al.). This figure is licensed under the Creative Commons Attribution 4.0 International License (CC BY). It has undergone minor technical enhancements in terms of clarity and legibility to meet journal standards. These modifications do not alter the original scientific content or data representation. For the full license terms, see https://creativecommons.org/licenses/by/4.0/ (accessed on 28 May 2026).

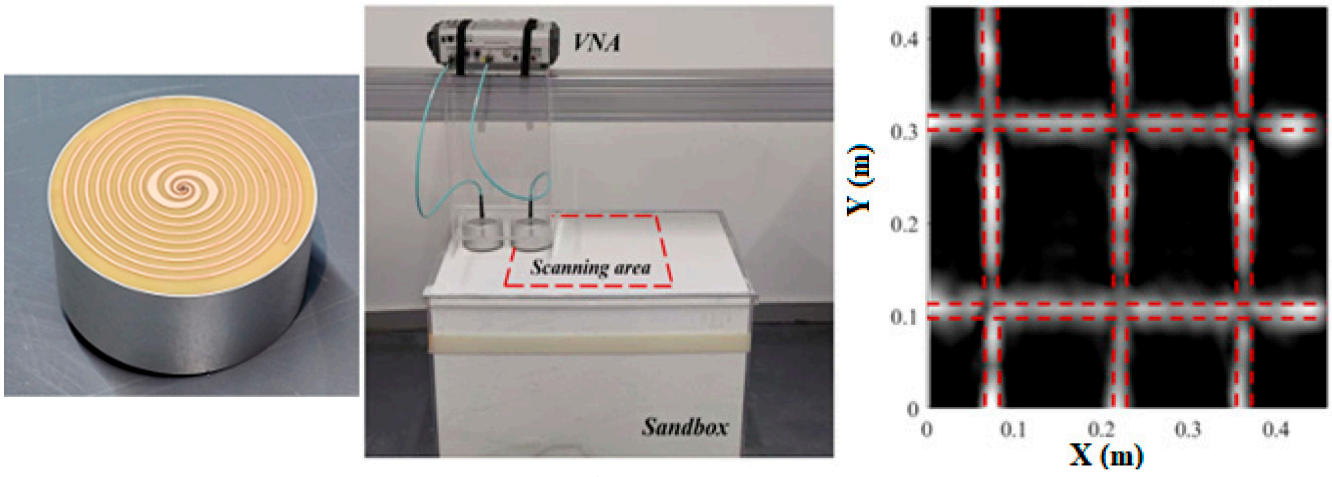

(**a**) (**b**) (**c**)

Figure 6. (**a**) Structure of the proposed antenna; (**b**) experimental measurement setup; and (**c**) image scan of the rebars. Reproduced from [55] (Copyright © 2025 H.Liu et al.). This figure is licensed under the Creative Commons Attribution 4.0 International License (CC BY). It has undergone minor technical enhancements in terms of clarity and legibility to meet journal standards. These modifications do not alter the original scientific content or data representation. For the full license terms, see https://creativecommons.org/licenses/by/4.0/ (accessed on 28 May 2026).

3. Comparative Analysis of GPR Antennas

Table 1 clearly highlights the fundamental trade-offs inherent in GPR antenna design. High-frequency wideband antennas, such as the Vivaldi with FSS [39] (1.7–40 GHz, 12.9 dBi), offer significantly higher gain but their penetration depth is limited to only very

shallow buried objects. A Vivaldi without FSS [40] (1.13–5 GHz, 10.89 dBi) achieves moderate penetration, while another Vivaldi design [41] (0.4–4 GHz, 12 dBi) is validated for buried object detection in Singapore soil. The tapered antenna with FSS reflector [52] (0.6–4.6 GHz, 7 dBi) stands out for its extremely compact size ($0.036\lambda \times 0.044\lambda \times 0.01\lambda$), although its penetration depth is not reported in the table. The spiral antenna [55] (1–6 GHz, gain not reported) targets detection of buried steel rebars, while the Vivaldi antenna [42] (0.5–3 GHz, 14.8 dBi) is designed for tree defect detection. In stark contrast, low-frequency antennas operating in the VHF and UHF bands (below 1 GHz)—including the dipole [47] (30–170 MHz, entirely within the VHF band), the envelope antenna [51] (140–510 MHz, spanning the upper VHF and lower UHF bands), and the bowtie [45] (0.25–0.85 GHz, covering both VHF and UHF)—enable very deep penetration, making them suitable for detecting tunnels, buried metallic plates in wet lossy soil, and pipes in roads or tunnel linings. However, this advantage comes at the cost of very low gain (dipole) or large electrical size (envelope: $0.28\lambda \times 0.28\lambda \times 0.07\lambda$; bowtie: $0.25\lambda \times 0.15\lambda \times 0.125\lambda$). Overall, no single antenna simultaneously satisfies all performance requirements: deeper penetration demands lower frequency and larger size, while high gain and wide bandwidth favor higher frequencies at the expense of depth. Consequently, antenna selection must be carefully tailored to the target application, whether for deep tunnel exploration, shallow high-resolution imaging, or detection in highly attenuating environments. To understand how each antenna type is applied to GPR, their key characteristics and drawbacks must be analyzed. Vivaldi antennas (with or without FSS) offer wide bandwidth and high gain, making them suitable for shallow, high-resolution surveys (e.g., buried object detection in Singapore soil or tree defect inspection). However, their penetration depth is limited, and they become electrically large at low frequencies. Bowtie antennas provide moderate bandwidth and gain with a relatively compact size; they are often used for deep penetration (e.g., detection of buried pipes in road and tunnel linings), but their gain is not considerable and they experience pattern distortion at low frequencies. Tapered antennas with FSS reflectors achieve wide bandwidth and a compact footprint, making them ideal for buried object detection; however, their gain is not as high as that of Vivaldi antennas with FSS, and their penetration depth is often unreported or limited. Dipole antennas are simple, low-cost, and operate at very low frequencies (VHF), enabling extremely deep penetration (e.g., tunnel detection in wet soil); their major drawbacks are very low gain (often <1 dBi) and omnidirectional radiation, which reduces spatial resolution. Spiral antennas are frequency-independent, offering wideband operation and suitability for detecting embedded metallic objects (e.g., steel rebars); however, they exhibit low gain and dispersion, and require absorbers to avoid back radiation. Envelope antennas operate in the VHF/UHF bands, providing deep penetration with moderate gain; their drawbacks include large physical size and complex feeding structures. This analysis shows that no single antenna excels in all GPR scenarios; the choice must balance gain, bandwidth, penetration depth, and form factor against the specific target and environment. It is also important to note the validation environment of these works. While most of the studies cited in Table 1 (e.g., [40–42,52,55]) validated their antennas only in controlled laboratory sandboxes, several have already performed realistic outdoor field tests. Specifically, Ref. [39] conducted GPR measurements outdoors in a prepared soil test field with metal sheets buried at depths of 1 and 2 inches, using a portable cart with VNA and a laptop for realistic field operation. Reference [45] performed both controlled laboratory measurements (basic radiation and time-domain analysis using a copper plate) and realistic outdoor field tests on a road with buried pipes and inside a tunnel lining, thereby bridging the gap between idealized validation and practical deployment. In [46], experiments were carried out outdoors using a drone-mounted GPR system over natural vegetation and a deeply buried tunnel (40 m), with the autonomous aerial vehicle flying

at 30 m altitude, confirming that the measurements are not laboratory-based. Likewise, ref. [47] validated the antenna in realistic outdoor/soil environments above grass-covered and sand-covered wet soil, as well as over a buried metallic plate for GPR imaging. Nevertheless, despite these notable exceptions, some of the reviewed studies remain confined to controlled, idealized conditions, typically using homogeneous or well-characterized media (e.g., dry sand, concrete, or wood), fixed antenna orientations, and absence of environmental interference. This leaves a partial gap between proof-of-concept demonstrations and actual field deployment. In real-world GPR surveys, antennas face highly variable and often hostile conditions: soil moisture content, temperature, and salinity can drastically alter the ground permittivity and conductivity, affecting impedance matching, propagation loss, and target contrast. Moreover, rough terrain, antenna wobble, proximity to metallic objects, and electromagnetic clutter from surrounding infrastructure are rarely replicated in a laboratory setting. These factors can degrade gain, distort radiation patterns, and introduce false targets or missed detections. Consequently, the reported performance metrics—gain, bandwidth, penetration depth—should be interpreted as upper bounds achievable under optimal conditions, not as guaranteed values in operational scenarios. Future work should therefore include systematic field trials with controlled environmental variations (e.g., wet vs. dry soil, different soil types, antenna elevation changes) and statistical robustness analysis. Only then can the true deployability of these antenna designs be assessed. This critical perspective does not diminish the value of the existing studies but rather highlights the essential next step toward practical GPR systems. Looking ahead, several emerging trends are expected to shape the next-generation of GPR antenna systems: metasurface-integrated and FSS-integrated designs for improved bandwidth, gain, front-to-back ratio, and reduced profile; reconfigurable and frequency-agile antennas (e.g., using PIN diodes or varactors) enabling multi-mode operation (switching between deep penetration and high resolution); additive manufacturing (3D printing) for rapid prototyping of complex dielectric lenses, conformal radomes, and fully printed antennas; miniaturization and flexible substrates for integration into handheld, drone-mounted, or wearable portable systems; and AI-assisted optimization and inversion for intelligent, real-time adaptive GPR operation.

Table 1. Comparative analysis of GPR antennas.

Ref	Year	Antenna Type	Size	Frequency Range/Fractional BW/Max. Gain	Penetration Depth	Real Application
[39]	2026	Vivaldi with FSS	$\lambda \times \lambda \times 0.008\lambda$	1.7–40 GHz/183.7%/12.9 dBi	50.8 mm	Detection of buried objects
[40]	2026	Vivaldi	$0.3\lambda \times 0.3\lambda \times 0.0061\lambda$	1.13–5 GHz/126.3%/10.8 dBi	377 mm	Buried object detection
[41]	2021	Vivaldi	$0.28\lambda \times 0.28\lambda \times 0.20\lambda$	0.4–4.0 GHz/163.6%/12 dBi	900 mm	Buried object detection in Singaporean soil
[42]	2024	Vivaldi	$0.29\lambda \times 0.29\lambda \times 0.48\lambda$	0.5–3 GHz/142.9%/14.8 dBi	100 mm	Tree defect detection on a Singapore rain tree trunk
[45]	2020	Bowtie	$0.25\lambda \times 0.15\lambda \times 0.125\lambda$	0.25–0.850 GHz/109.1%/4 dBi	2000 mm	Detection of Buried Pipes in Road and Tunnel Linings
[46]	2025	Dipole	$0.47\lambda \times 0.04\lambda$	30–170 MHz/140%/0.3 dBi	40,000 mm	Detection of an underground tunnel with an autonomous aerial vehicle

Table 1. *Cont.*

Ref	Year	Antenna Type	Size	Frequency Range/Fractional BW/Max. Gain	Penetration Depth	Real Application
[47]	2020	Envelope	0.28λ × 0.28λ × 0.07λ	140–510 MHz/113.8%/6.5 dBi	600 mm	Buried metallic plate detection in wet lossy soil
[52]	2021	Tapered with FSS reflector	0.036λ × 0.044λ × 0.01λ	0.6–4.6 GHz/153.8%/7 dBi	Not reported	Buried object detection in a sand tank
[55]	2025	Spiral	0.37λ × 0.37λ × 0.173λ	1–6 GHz/142.9%/Not reported	120 mm	Detection of buried steel rebars

4. Conclusions

This review examined advanced antenna technologies validated in experimental GPR systems, covering six distinct categories: Vivaldi, bowtie, tapered, dipole, spiral, and envelope. The findings underscore fundamental trade-offs inherent to GPR antenna design. High-frequency wideband antennas—such as the Vivaldi with FSS (1.7–40 GHz, 12.9 dBi)—deliver high gain but restrict penetration to very shallow targets. Similarly, the tapered antenna with an FSS reflector achieves wide bandwidth and reasonable gain with an extremely compact footprint, although its penetration depth is not reported. The spiral antenna (1–6 GHz) targets buried steel rebar detection. These designs prioritize resolution and gain over depth. In stark contrast, low-frequency designs (below 1 GHz)—including the dipole (30–170 MHz, 0.3 dBi), the envelope antenna (140–510 MHz, 6.5 dBi), and the bowtie (0.25–0.85 GHz, 4 dBi)—enable very deep penetration, making them ideal for detecting tunnels, buried metallic plates in wet lossy soil, and pipes in roads or tunnel linings. However, this comes at the cost of very low gain (dipole) or large physical size (envelope and bowtie). The bowtie provides a moderate gain compromise, while larger envelope antennas improve penetration in lossy media at the expense of portability. Crucially, no single antenna simultaneously meets all performance criteria; optimal selection is inherently application-driven, depending on whether deep penetration, high resolution, or operation in attenuating environments is prioritized. Persistent challenges include achieving further miniaturisation without degrading performance, ensuring stable operation in heterogeneous and lossy subsurface conditions, and developing robust, manufacturable designs suitable for real-world deployment. Looking ahead, future research is expected to prioritise intelligent and adaptive antenna systems, with artificial intelligence playing a transformative role in antenna synthesis, parameter optimisation, and real-time adaptive GPR operation. Specific machine learning techniques are already showing promise in this domain. For instance, neural networks can be trained to optimize complex antenna geometries (e.g., FSS unit cells or tapered slot profiles) by learning the mapping between design parameters and electromagnetic performance, dramatically reducing simulation time. Likewise, deep learning models have been successfully applied to inverse scattering problems in GPR, where neural networks reconstruct subsurface dielectric profiles from measured scattered fields, enabling faster and more accurate target identification. Integrating such AI-driven optimisation and inversion methods directly into adaptive GPR systems represents a concrete pathway toward fully intelligent, field-deployable antennas. Ultimately, this review provides researchers and practitioners with a structured reference that summarizes recent GPR antenna designs and their suitability for different applications, guided by the needed penetration depth.

Author Contributions: Conceptualization, A.C.; methodology, A.C., D.A., L.C. and G.A.; formal analysis, A.C., D.A., L.C. and G.A.; investigation, A.C. and D.A.; resources, D.A., L.C. and G.A.; data curation, A.C.; writing—original draft preparation, A.C., D.A. and L.C.; writing—review and editing, A.C., D.A. and L.C.; visualization, D.A., L.C. and G.A.; supervision, G.A. All authors have read and agreed to the published version of the manuscript.

Funding: This research received no external funding.

Data Availability Statement: The original contributions presented in the study are included in the article; further inquiries can be directed to the corresponding author.

Acknowledgments: The authors gratefully acknowledge the support of the LTSS and LAADI laboratories of the University of Djelfa.

Conflicts of Interest: The authors declare no conflicts of interest.

References

1. Edemsky, D.; Popov, A.; Prokopovich, I.; Garbatsevich, V. Airborne Ground Penetrating Radar, Field Test. *Remote Sens.* **2021**, *13*, 667. [CrossRef]
2. Chaabane, A.; Guerroui, M. Circularly Polarized Ultra Wideband Antenna with Question Mark-Shaped Patch for Ground Penetrating Radar Applications. *J. Appl. Res. Technol.* **2022**, *20*, 274–283. [CrossRef]
3. Guerroui, M.; Chaabane, A.; Boualleg, A. Super UWB Grooved and Corrugated Antenna for GPR Application. *Period. Polytech. Electr. Eng. Comput. Sci.* **2022**, *66*, 31–37. [CrossRef]
4. Morozov, P.; Morozov, F.; Lazarev, M.; Bogolyubov, L.; Popov, A. Characterization of Antenna Radiation Pattern and Penetration Depth in Ground Penetrating Radar Field Missions. *Remote Sens.* **2023**, *15*, 5452. [CrossRef]
5. Comite, D.; Galli, A.; Catapano, I.; Soldovieri, F. The Role of the Antenna Radiation Pattern in the Performance of a Microwave Tomographic Approach for GPR Imaging. *IEEE J. Sel. Top. Appl. Earth Obs. Remote Sens.* **2017**, *10*, 4337–4347. [CrossRef]
6. Chaabane, A.; Guerroui, M. Printed UWB Rhombus Shaped Antenna for GPR Applications. *Iran. J. Electr. Electron. Eng.* **2021**, *17*, 2041. [CrossRef]
7. De Benedetto, D.; Quarto, R.; Castrignanò, A.; Palumbo, D.A. Impact of Data Processing and Antenna Frequency on Spatial Structure Modelling of GPR Data. *Sensors* **2015**, *15*, 16430–16447. [CrossRef]
8. Sangpet, P.; Chanwattanapong, W.; Sangmook, C.; Mahatthanajatuphat, C.; Jangjing, T.; Chudpooti, N. Design of Ultra-Wideband Antipodal Vivaldi Antenna with Improving Impedance Matching using Elliptical Stub for GPR Applications. In Proceedings of the 13th International Electrical Engineering Congress (iEECON), Hua Hin, Thailand, 5–7 March 2025; pp. 1–4. [CrossRef]
9. Guerroui, M.; Chaabane, A.; Ikni, S.; Boualleg, A.; Guebgoub, N.; Mahri, O. A Printed U-Shaped Coplanar Waveguide Feed UWB Antenna for GPR Applications. *Adv. Electromagn.* **2022**, *11*, 51–59. [CrossRef]
10. Wang, Z.; Ye, S.; Xu, Y.; Zhu, M.; Ji, Y.; Liu, X.; Fang, G.; Fang, Y. A Coherent Difference Imaging Method for Antenna Decoupling in Ground-Penetrating Radar. *Electronics* **2026**, *15*, 893. [CrossRef]
11. Chaabane, A.; Babouri, A. Dual Band Notched UWB MIMO Antenna for Surfaces Penetrating Application. *Adv. Electromagn.* **2019**, *8*, 6–15. [CrossRef]
12. Gupta, K.; Anjitha, V.; Asok, A.O.; Dey, S. Design of an Ultra-wideband Antipodal Vivaldi Antenna for Deep Ground Penetration and High-Resolution Through-Wall Imaging. In Proceedings of the IEEE Space, Aerospace and Defence Conference (SPACE), Bangalore, India, 21–23 July 2025; pp. 1–5. [CrossRef]
13. Shome, P.P.; Khan, T.; Kanaujia, B.K.; Kishk, A.A.; Antar, Y.M.M. Unidirective Miniaturized, Ultrawideband Antenna for Sensing Buried Objects in Handheld Ground-Penetrating Radar Systems: A Design Approach. *IEEE Antennas Propag. Mag.* **2023**, *65*, 46–55. [CrossRef]
14. Aboudourib, A.; Serhir, M.; Lesselier, D. A Processing Framework for Tree-Root Reconstruction Using Ground-Penetrating Radar Under Heterogeneous Soil Conditions. *IEEE Trans. Geosci. Remote Sens.* **2021**, *59*, 208–219. [CrossRef]
15. Pi, S.; Wang, T.; Lin, J. Directional and High-Gain Ultra-Wideband Bow-Tie Antenna for Ground-Penetrating Radar Applications. *Remote Sens.* **2023**, *15*, 3522. [CrossRef]
16. Saeidi, T.; Alhawari, A.R.H.; Almawgani, A.H.M.; Alsuwian, T.; Imran, M.A.; Abbasi, Q. High Gain Compact UWB Antenna for Ground Penetrating Radar Detection and Soil Inspection. *Sensors* **2022**, *22*, 5183. [CrossRef]
17. Warren, C.; Giannopoulos, A. Investigation of the directivity of a commercial Ground-Penetrating Radar Antenna using a Finite-Difference Time-Domain antenna model. In Proceedings of the 14th International Conference on Ground Penetrating Radar (GPR), Shanghai, China, 4–8 June 2012; pp. 226–231. [CrossRef]
18. Mohammad, Z.; Chrysler, A.M. Airborne Reflector-Based Ground Penetrating Radar for Environmental and Archaeological Studies. *IEEE Open J. Antennas Propag.* **2023**, *4*, 748–753. [CrossRef]

19. Kalita, A.J.; Barkataki, N.; Sarma, U. Design and Optimisation of Inverted U-Shaped Patch Antenna for Ultra-Wideband Ground-Penetrating Radar Applications. *Eng. Proc.* **2025**, *87*, 25. [CrossRef]
20. Kundu, S.; Chatterjee, A.; Jana, S.K.; Parui, S.K. A Compact Umbrella-Shaped UWB Antenna with Gain Augmentation Using Frequency Selective Surface. *Radioengineering* **2018**, *27*, 448–454. [CrossRef]
21. Hu, R.; Zhang, F.; Ye, S.; Fang, G. Ultra-Wideband and High-Gain Vivaldi Antenna with Artificial Electromagnetic Materials. *Micromachines* **2023**, *14*, 1329. [CrossRef] [PubMed]
22. Jol, H.M. *Ground Penetrating Radar Theory and Applications*; Elsevier: Amsterdam, The Netherlands, 2009; ISBN 978-0-444-53348-7. [CrossRef]
23. Joula, M.; Rafiei, V.; Karamzadeh, S. High gain UWB Bow-Tie Antenna Design for Ground Penetrating Radar Application. *Microw. Opt. Technol. Lett.* **2018**, *60*, 2425–2429. [CrossRef]
24. Serhir, M.; Lesselier, D. Wideband Reflector-Backed Folded Bowtie Antenna for Ground Penetrating Radar. *IEEE Trans. Antennas Propag.* **2018**, *66*, 1056–1063. [CrossRef]
25. Nayak, R.; Maiti, S. A Review of Bow-Tie Antennas for GPR Applications. *IETE Tech. Rev.* **2019**, *36*, 382–397. [CrossRef]
26. Guo, L.; Yang, H.; Zhang, Q.; Deng, A.M. A Compact Antipodal Tapered Slot Antenna With Artificial Material Lens and Reflector for GPR Applications. *IEEE Access* **2018**, *6*, 44244–44251. [CrossRef]
27. Kundu, S.; Chatterjee, A. Sharp Triple-Notched Ultra Wideband Antenna with Gain Augmentation Using FSS for Ground Penetrating Radar. *Wirel. Pers. Commun.* **2021**, *117*, 1399–1418. [CrossRef]
28. Cheng, H.; Yang, H.; Li, Y.; Chen, Y. A Compact Vivaldi Antenna With Artificial Material Lens and Sidelobe Suppressor for GPR Applications. *IEEE Access* **2020**, *8*, 64056–64063. [CrossRef]
29. Zheng, W.; Luo, W.; Hao, T. Experimental Investigations on Enhanced GPR Detection Assisted by Broadband Metasurfaces. *IEEE Trans. Instrum. Meas.* **2024**, *73*, 1004911. [CrossRef]
30. Bousbaa, W.; Medkour, H.; Bouttout, F.; Zoubeida Messali, Z. Fully Planar Frequency Independent Square Archimedean Spiral Antenna with Impedance Transformer for Ground Penetrating Radars. *Microw. Opt. Technol. Lett.* **2021**, *63*, 295–309. [CrossRef]
31. Elsherbini, A.; Sarabandi, K. ENVELOP Antenna: A Class of Very Low Profile UWB Directive Antennas for Radar and Communication Diversity Applications. *IEEE Trans. Antennas Propag.* **2013**, *61*, 1055–1062. [CrossRef]
32. Sutham, T.; Thaiwirot, W.; Akkaraekthalin, P. Design of Ultra-Wideband Inverted U-Shaped Slot Antenna with Reflector for GPR Applications. In Proceedings of the 19th International Conference on Electrical Engineering/Electronics, Computer, Telecommunications and Information Technology (ECTI-CON), Prachuap Khiri Khan, Thailand, 24–27 May 2022; pp. 1–4. [CrossRef]
33. Ali, J.; Abdullah, N.; Ismail, M.Y.; Mohd, E.; Shah, S.M. Ultra-Wideband Antenna Design for GPR Applications: A Review. *Int. J. Adv. Comput. Sci. Appl.* **2017**, *8*. [CrossRef]
34. Kumar, G.; Mevada, P.; Singh, V.K.; Mahajan, M. Compact Dual Polarized Ultrawideband (UWB) Antipodal Vivaldi Antenna for Rover Based GPR System. In Proceedings of the 2022 IEEE MAPCON, Bangalore, India, 12–16 December 2022; pp. 287–291. [CrossRef]
35. Zou, X.-J.; Wang, Y.-W.; Zong, B.-F.; Xu, X.-G.; Han, L.-X.; Zhu, H.; Song, W.; Tan, M.; Du, H.-N. Miniaturized Low-Profile Ultrawideband Antipodal Vivaldi Antenna Array Loaded With Edge Techniques. *IEEE Trans. Antennas Propag.* **2026**, *74*, 1156–1161. [CrossRef]
36. Caliskan, A.; Hoşgör, Y.; Turk, A.S.; Kizilay, A. Partially Dielectric Loaded Planar Vivaldi Array Antenna for Forward-Looking GPR Applications. *Microw. Opt. Technol. Lett.* **2024**, *66*, e33928. [CrossRef]
37. Guo, J.; Tong, J.; Zhao, Q.; Jiao, J.; Huo, J.; C. Ma, C. An Ultrawide Band Antipodal Vivaldi Antenna for Airborne GPR Application. *IEEE Geosci. Remote Sens. Lett.* **2019**, *16*, 1560–1564. [CrossRef]
38. Shen, F.; Yang, N.; Xia, C.; Wan, T.; Kang, J. A Compact Aperture-Slot Antipodal Vivaldi Antenna for GPR Systems. *Sensors* **2026**, *26*, 810. [CrossRef]
39. Das, P.; Deepak, A.; Nithin, V.; Kundu, S. A Dual-Band Circularly Polarised Antipodal Vivaldi Antenna for Subsurface Scanning. *Results Eng.* **2026**, *29*, 109448. [CrossRef]
40. Riyanti, K.P.K.; Setijadi, E.; Hendrantoro, G.; Nurhayati, N. CPW feed and stub optimization for Vivaldi antennas in broadband ground-penetrating radar applications. *AEU-Int. J. Electron. Commun.* **2026**, *207*, 156219. [CrossRef]
41. Sun, H.-H.; Lee, Y.H.; Luo, W.; Ow, L.F.; Yusof, M.L.M.; Yucel, A.C. Compact Dual-Polarized Vivaldi Antenna with High Gain and High Polarization Purity for GPR Applications. *Sensors* **2021**, *21*, 503. [CrossRef]
42. Cheng, K.; Lee, Y.H.; Qian, J.; Lee, D.; Yusof, M.L.M.; Yucel, A.C. A Compact Dual-Polarized Vivaldi Antenna with High Gain for Tree Radar Applications. *Sensors* **2024**, *24*, 4170. [CrossRef] [PubMed]
43. Wu, Y.; Shen, F.; Yuan, Y.; Xu, D. An Improved Modified Universal Ultra-Wideband Antenna Designed for Step Frequency Continuous Wave Ground Penetrating Radar System. *Sensors* **2019**, *19*, 1045. [CrossRef]

44. Kumar, G.; Mevada, P.; Gupta, R.C.; Singh, V.K.; Mahajan, M.B. Compact Linearly Polarized Resistor Loaded Bow-Tie Antenna for GPR System. In Proceedings of the IEEE Microwaves, Antennas, and Propagation Conference (MAPCON), Hyderabad, India, 9–13 December 2024; pp. 1–5. [CrossRef]
45. Yang, G.; Ye, S.; Ji, Y.; Zhang, X.; Fang, G. Radiation Enhancement of an Ultrawideband Unidirectional Folded Bowtie Antenna for GPR Applications. *IEEE Access* **2020**, *8*, 182218–182228. [CrossRef]
46. Wang, Z.; Ye, S.; Lu, W.; Song, C.; Ji, Y.; Fang, G. A Dual H-Shaped Ultrawideband Antenna for AAV-Based Ground Penetrating Radar. *IEEE Antennas Wirel. Propag. Lett.* **2025**, *24*, 12. 4610–4614. [CrossRef]
47. Yektakhah, B.; Chiu, J.; Faisal Alsallum, F.; Sarabandi, K. Low-Profile, Low-Frequency, UWB Antenna for Imaging of Deeply Buried Targets. *IEEE Geosci. Remote Sens. Lett.* **2020**, *17*, 1168–1172. [CrossRef]
48. Kundu, S. High Gain Compact Ultra-Wideband "Antenna Frequency Selective Surface" and its Performance Evaluation in Proximity of Soil Surface. *Microw. Opt. Technol. Lett.* **2021**, *63*, 869–875. [CrossRef]
49. Mahouti, P.; Kīzīlay, A.; Razevig, V.V.; Belen, M.A.; Piltan, O.C. Vivaldi Antenna Design With Frequency Selective Surfaces for GPR Applications. In Proceedings of the 2023 10th International Conference on Recent Advances in Air and Space Technologies (RAST), Istanbul, Turkiye, 7–9 June 2023; pp. 1–4. [CrossRef]
50. Ud Din, I.; Ullah, S.; Naqvi, S.I.; Ullah, R.; Ullah, S.; Ali, E.M.; Alibakh-shikenari, M. Improvement in the Gain of UWB Antenna for GPR Applications by Using Frequency-Selective Surface. *Int. J. Antennas Propag.* **2022**, *2022*, 2002552. [CrossRef]
51. Al-Gburi, A.J.A.; Ibrahim, I.B.M.; Zeain, M.Y.; Zakaria, Z. Compact Size and High Gain of CPW-Fed UWB Strawberry Artistic Shaped Printed Monopole Antennas Using FSS Single Layer Reflector. *IEEE Access* **2020**, *8*, 92697–92707. [CrossRef]
52. Ksouri, E.; Boufrioua, A.; Belazzoug, M.; Messaoudene, I.; Melouki, N.; Denidni, T.A. A gain enhancement of compact UWB antenna based on a single FSS layer. *Microw. Opt. Technol. Lett.* **2024**, *66*, e34301. [CrossRef]
53. Sen, G.; Das, S. Interdigital Coupled Compact FSS Reflector for UWB Antenna Gain Enhancement. *Prog. Electromagn. Res. C* **2024**, *120*, 47–52. [CrossRef]
54. Raza, A.; Lin, W.; Ishfaq, M.K.; Inam, M.; F. Masud, F.; Dahri, M.H. A Wideband Reflector-Backed Antenna for Applications in GPR. *Int. J. Antennas Propag.* **2021**, *2021*, 3531019. [CrossRef]
55. Liu, H.; Zhang, S.; Wu, P.; Meng, X.; Zhou, J.; Du, Y. A Circularly Polarized Broadband Composite Spiral Antenna for Ground Penetrating Radar. *Sensors* **2025**, *25*, 1890. [CrossRef] [PubMed]